frontiers | Frontiers in Energy Research

TYPE Original Research
PUBLISHED 29 August 2022
DOI 10.3389/fenrg.2022.960786

OPEN ACCESS

EDITED BY
Fei Zhang,
The Chinese University of Hong Kong, Shenzhen, China

REVIEWED BY
Lingqi Huang,
Zhejiang University of Science and Technology, China
Tong Liu,
Hong Kong Polytechnic University, Hong Kong SAR, China

*CORRESPONDENCE
K. Wenelska,
kwenelska@zut.edu.pl

SPECIALTY SECTION
This article was submitted to Electrochemical Energy Conversion and Storage, a section of the journal Frontiers in Energy Research

RECEIVED 03 June 2022
ACCEPTED 14 July 2022
PUBLISHED 29 August 2022

CITATION
Wenelska K, Adam V, Thauer E, Singer L, Klingeler R, Chen X and Mijowska E (2022), Fabrication of 3D graphene/MoS_2 spherical heterostructure as anode material in Li-ion battery. *Front. Energy Res.* 10:960786. doi: 10.3389/fenrg.2022.960786

Fabrication of 3D graphene/MoS_2 spherical heterostructure as anode material in Li-ion battery

K. Wenelska[1]*, V. Adam[2], E. Thauer[2], L. Singer[2], R. Klingeler[2,3], X. Chen[1] and E. Mijowska[1]

[1]Szczecin Faculty of Chemical Technology and Engineering, Department of Nanomaterials Physicochemistry, West Pomeranian University of Technology, Szczecin, Poland, [2]Kirchhoff Institute of Physics, Heidelberg University, Heidelberg, Germany, [3]Centre for Advanced Materials (CAM), Heidelberg University, Heidelberg, Germany

Three-dimensional (3D) graphene-based nanocomposites have received considerable attention in both fundamental research and industrial applications, as they combine the functionalities of well-controlled nano-architectures and the integrity of bulk materials. Actually, among these materials, spherical structures are attracting more and more attention worldwide due to their excellent performance in various fields such as drug delivery, heterogeneous catalysis, encapsulation of support, and electrode materials for lithium-ion batteries. Herein, a facile route to fabricate a three-dimensional hierarchical graphene/MoS_2 nanocomposite is presented. The molecular heterostructure is derived from graphene oxide flakes and precursors of molybdenum ($(NH_4)_2Mo_7O_4{\cdot}4H_2O$) and sulfur (L-cysteine). Spherical morphology (GO/MoS_2) is obtained *via* self-assembly of the precursor. This 3D nanocomposite exhibits MoS_2-nanosheets strongly linked to graphene oxide flakes, which renders it particularly suited to exploit the conversion reaction of MoS_2 for electrochemical energy storage. When assembled into an electrode in lithium-ion batteries, as-prepared GO/MoS_2 electrodes indeed deliver a high initial charge capacity of 783 mA h g^{-1} at a current density of 100 mA/g and Coulombic efficiency of more than 96% from the second cycle on exceeding the theoretical capacity of the pristine 2D MoS_2 and graphene. Overall, the study sheds some light on the design of 3D heterostructure as a promising anode material in Li-ion batteries.

KEYWORDS

molybdenum disulfide (MoS) 2, graphene, lithium-ion batteries, electrochemistry (113), anode

Introduction

Motivated by recent rapid advancements and considering the constraints of two-dimensional (2D) graphene, the research on graphene-based materials has been directed toward the exploration of different graphene-like morphologies, with appropriate and attractive contributions from physics, chemistry, and materials science, among others (Novoselov et al., 2004; Novoselov et al., 2005; Zhu et al., 2014). The actual application

performance achieved using 2D materials is always less than that anticipated based on its ideal properties such as high surface area, high charge carrier mobility, premier mechanical strength, and excellent thermal conductivity.

Functional carbon nanospheres with controllable size, surface area, pore diameter, surface morphology, and chemical composition are an appealing topic. They reveal enhanced performance in a wide variety of applications, such as electrode materials for electrochemical energy storage, absorbents, or catalysts (Zheng et al., 2014; Wang et al., 2021). Graphene spheres and reshaped structures with good chemical and mechanical properties are among the most promising candidates to overcome the obstacles associated with 2D nanosheets. They exhibit plentiful porous channels with enhanced electrical conductivity and superb structural stability (Liu et al., 2020a; Ji et al., 2020).

Various nanostructured MoS_2 and carbon composites have triggered intensive interest due to their intriguing physicochemical properties. Hou et al. reported molybdenum disulfide nanoparticles with spherical structures prepared *via* a hydrothermal method of about 190 nm in diameter (Koroteev et al., 2021). Cui and co-workers prepared a novel carbon-coated MoS_2 nanobowl structure by a solvothermal method, followed by an annealing process (Cui et al., 2015). Zhou et al. reported on carbon nanofibers decorated with molybdenum disulfide sheets (Liu et al., 2020b). To optimize links between MoS_2 and carbon, a variety of approaches have been explored, such as exploiting the high wettability of N-doped graphitic surface and electrostatic attraction between thiomolybdate precursor anion and N-doped sites to fabricate amorphous molybdenum sulfide layers directly bound at vertical N-doped carbon nanotube forest surface (Li et al., 2014; Long et al., 2014). Further approaches have yielded MoS_2@C nanotubes (Zhang et al., 2016a), C/MoS_2/C sandwiched hollow spheres (Li et al., 2017), carbon-sheathed MoS_2 on CNT (Zhang et al., 2018), and MoS_2/N-doped carbon porous nanorods.

A particularly promising application of MoS_2/C composite heterostructures is testing them as anode material in lithium-ion batteries (LIB). While their unique and layered structure and high theoretical lithium storage capacity of 670 mA h g^{-1} imply great prospects of MoS_2 for LIB in general (Gao et al., 2013; Hu et al., 2016), semi-conductivity and large volume changes associated with the conversion reaction process are severe drawbacks for the actual application (Stephenson et al., 2014). Increasing conductivity and mechanical strength by fabrication of 3D MoS_2/C composite structures have, however, resulted in various materials with good cycling stability in LIB (Zhang et al., 2016a; Zhang et al., 2018; Li et al., 2019a) and sodium-ion batteries (David et al., 2018; Xiong et al., 2018; Li et al., 2019b). In particular, structures are expected to offer several benefits (Li et al., 2009; Wu et al., 2018). The proposed 3D heterostructures exhibit a high contact area with the electrolyte providing more active sites for de-/lithiation and favorable Li^+ transport kinetics. Also, it is proposed that the internal cross-linkage of nanosheets can prevent their aggregation and ensure good structural stability.

We present a facile and highly reproducible route to prepare a spherical 3D structure based on graphene and MoS_2 in a solution phase. MoS_2 and graphene oxide were self-assembled from structures to spherical heterostructures at a high-temperature reaction in a line-Teflon autoclave. A mechanism for reshaping the spherical structure is proposed. Furthermore, we report on the electrochemical performance of designed GO/MoS_2-based when used as electrodes in Li-ion battery.

Experimental section

Preparation of graphene oxide

The graphene oxide was synthesized by a modified Hummers method (Hummers and Offeman, 1958). Shortly, 1 g of graphite was mixed with 6 g of $KMnO_4$ in a flask. Concentrated sulfur acid and orthophosphoric acid (90:10 ml) were added to the flask and then heated to 50°C while stirring. After 24 h, the mixture was poured into ice (100 ml) and H_2O_2 (30%, 1 ml) and then filtered using a polycarbonate membrane. The solid product was washed twice with water, 10% HCl, and ethanol and, finally, vacuum-dried for 12 h.

Preparation of MoS_2 and GO-based heterostructures (GO/MoS_2)

A total of 30 mg of GO was introduced to 820 mg of ammonium molybdate tetrahydrate $(NH_4)_2Mo_7O_4{\bullet}4H_2O$ mixed with 120 ml of DI water and sonicated for 30 min. In the next step, a source of sulfur (2.4 g of l-cysteine) was added. The mixture was transferred into a Teflon-lined steel autoclave and heated to 240°C for 24 h. Afterward, the sample was washed with ethanol and dried at 60°C for 24 h.

Characterization

The crystallographic information regarding the as-synthesized samples was established by X-ray diffraction (XRD), performed using Philips X'Pert PRO X-ray diffractometer a Cu Ka radiation. The morphology of the samples was obtained using transmission electron microscopy (Tecnai F20-based at 200 kV) and scanning electron microscopy (TESCAN VEGA 3). For monitoring the microstructural changes of the GO/MoS_2-electrode after cycling, *ex situ* SEM studies were performed using a JEOL JSM-7610F scanning electron microscope. The cycled electrodes were disassembled in an Argon glove box, washed with ethylene carbonate, and then

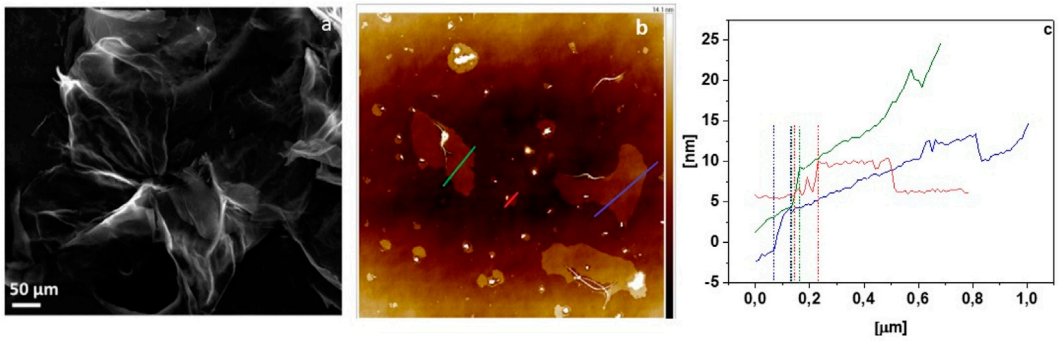

FIGURE 1
SEM image **(A)**, AFM image **(B),** and height profile **(C)** of GO flakes.

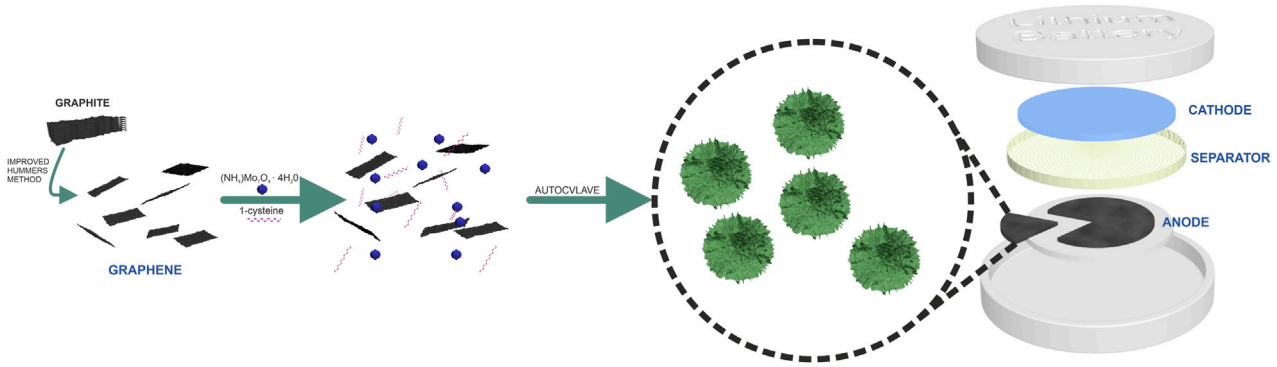

SCHEME 1
Schematic illustration of synthesis and application of GO/MoS_2.

dried overnight. Atomic Force Microscopy (AFM NTEGRA Aura (NT-MTD) microscope) was employed to obtain the thickness and number of layers of GO. Thermogravimetric analysis (TGA) was carried out using an SDT Q6000 thermoanalyzer instrument (TA Instruments Inc.) under airflow of 100 ml/min. The samples were heated from room temperature to 900°C at a linear heating rate of 10°C/min. Raman spectroscopy was applied with a microscope mode (InViaRenishaw) with a 785 nm laser. N_2 adsorption/desorption isotherms were obtained at liquid nitrogen temperature (77 K) using a Micromeritics ASAP 2010M instrument. The Brunauer–Emmett–Teller (BET) and Barrett–Joyner–Halenda (BJH) methods were adopted to calculate the specific surface area and pore size distribution.

Electrochemical studies on GO/MoS_2 have been performed by means of Swagelok-type cells (Ottmann et al., 2015) at 25°C. Working electrodes were prepared by mixing 80 wt% active material, 10 wt% carbon black (Super C65, Timcal), and 10 wt% polyvinylidene fluoride (PVDF, Sigma-Aldrich, 99%) in anhydrous 1-methyl-2-pyrrolidinone (NMP, Sigma-Aldrich, 99%) for 12 h. After pasting the slurry on a circular copper mesh of 10 mm diameter, the electrodes were vacuum dried overnight at 65°C and pressed subsequently. The procedure resulted in an active mass loading of about 4 mg cm^{-2}. The cells were assembled in an Ar-Glovebox using the as-prepared working electrodes, two layers of glass fiber (Whatman GF/D) as a separator and lithium foil pressed on a nickel plate as a counter electrode. A total of 200 µL of a 1 M $LiPF_6$ salt solution in 1:1 ethylene carbonate (EC) and dimethyl carbonate (DMC) (Merck Electrolyte LP30) was used as the electrolyte. Electrochemical measurements were performed between 0.01 and 3.0 V *versus* Li/Li^+ at a scan rate of 0.05 mV/s for cyclic voltammetry and 100 mA/g as the

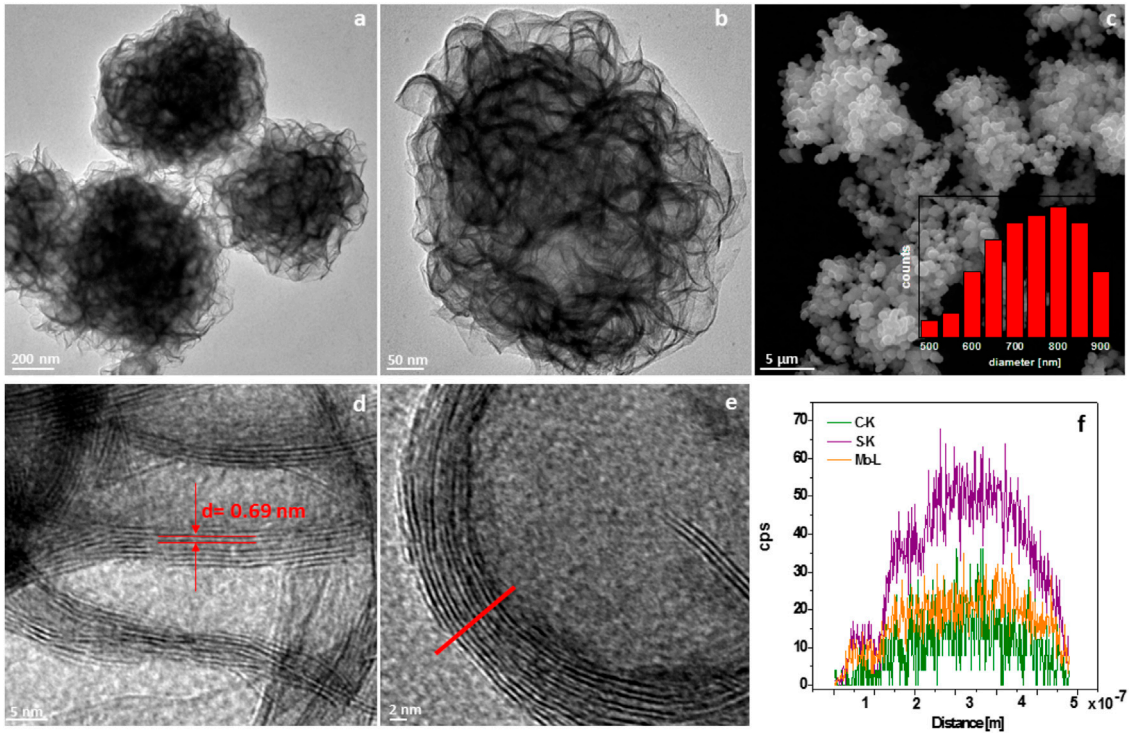

FIGURE 2
TEM images **(A,B)**, SEM image **(C)**, HRTEM images **(D,E),** and line profile **(F)** of GO/MoS_2.

current rate for galvanostatic cycling using a VMP3 multichannel potentiostat (Bio-Logic SAS). The carbon content was examined by elemental analysis using Vario MICRO Cubes (Elementar).

Results and discussion

The morphology of GO investigated by SEM and AFM microscopes is presented in Figures 1A,B, respectively. Figure 1A shows that few-layered GO was successfully obtained by a modified Hummers method. The Tapping-mode of AFM used to determine the thickness of GO (Figure 1C) implies a thickness of ~4.3–5.4 nm of the resulting sheets corresponding to 7–9 layers of GO (Wang et al., 2017).

The schematic illustration of synthesis and the application for GO/MoS_2 is present in Scheme 1.

Figure 2 shows TEM and SEM images of the obtained spherical material. Specifically, Figures 2A,B present the TEM images of structure based on GO and MoS_2 (GO/MoS_2). The SEM image (Figure 2C) reveals that the composite is in the form of irregular spheres with diameters of ~800 ± 70 nm. Further investigations by means of TEM (Figures 2A,C) allow determining the morphology in greater detail. The irregular spheres are formed by flowerlike structures. A high-resolution transmission electron microscopy image (Figures 2D,E) enables reading off the distance between the layers to be 0.69 nm which is slightly larger than the (002) plane spacing of 0.62 nm in bulk MoS_2. As shown in Figure 2F, EDS line scans taken across the wall of the sphere (see red line in Figure 2E clearly prove the elemental composition: C, Mo, and S are evenly distributed throughout the wall.

TGA studies performed in the temperature range from 25 to 1,000°C under air gas flow (Figure 3A) observed a gradual weight loss occurring in three steps. A first weight loss of 9% observed in the range of 320–400°C is associated with oxidation of MoS_2 to MoO_3. The next significant weight loss of 58% appears above 680°C and corresponds to graphite burning. After burning at around 900°C, the ash content in the ceramic cap is about 1.5%, corresponding to MoO_3.

The presence of crystalline MoS_2 in GO/MoS_2 is revealed by powder XRD as shown in Figure 3B. The diffraction peaks at 2Θ of 14°, 33°, 39°, and 59.8° can be unambiguously assigned to the (002), (100), (103), and (110) planes in hexagonal MoS_2, respectively (Zhang et al., 2016b). The (002) peak indicates the formation of the well-stacked layered structure of MoS_2 (Chhowalla and Amaratunga, 2000).

No obvious XRD peaks from a carbon phase are detected, which might be due to its lower content (<10 wt%), its rather

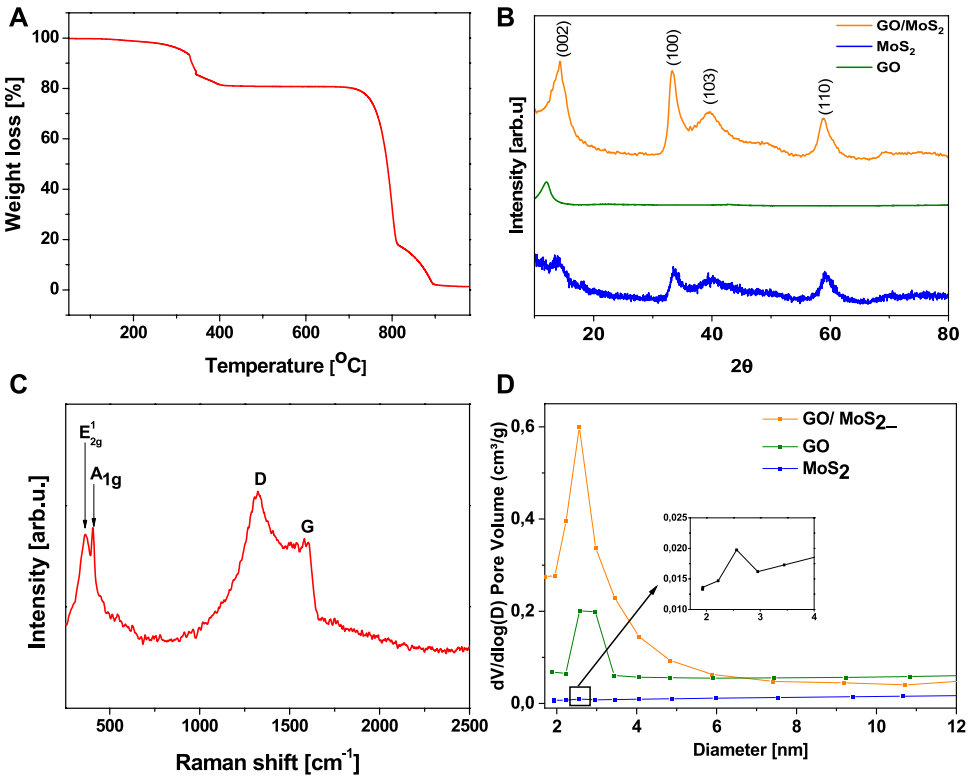

FIGURE 3
TGA profile **(A)**, XRD pattern **(B)**, Raman spectrum **(C)** and BJH pore size distribution of GO, MoS_2, and GO/MoS_2 **(D)**.

amorphous nature, and the high background signal. The presence of carbon is, however, confirmed *via* Raman spectroscopy (Figure 3C), which is one of the most sensitive techniques to characterize carbon materials. The spectrum shows the G-mode at about 1,583 cm^{-1} arising from the stretching of the C-C bond in graphitic materials, and it is common to all sp^2-carbon systems (Novoselov et al., 2004), whereas the D band at about 1,353 cm^{-1} is assigned the so-called breathing vibrations, which are mainly enabled by defects and disorder. Raman data of GO/MoS_2 present strong signals of $E_{2g}{}^1$ and A_{1g} modes of MoS_2 (Wieting and Verble, 1971).

The surface area and pore volume of GO/MoS_2 andthe intermediate products, i.e., the pure GO flakes and exfoliated MoS2 are presented on Figure 3D. The nanocomposite GO/MoS_2 features the largest surface area of 68 m^2/g. For the pure GO flakes and exfoliated MoS_2, much smaller surface areas of 10 and 11 m^2/g were observed, respectively. The pore volume in GO/MoS_2 is strongly enhanced to 0.52 cm^3/g, whereas GO and the exfoliated MoS_2 exhibit pore volumes of 0.002 and 0.01 cm^3/g, correspondingly. According to the pore distribution of the three materials calculated by means of the Barrett–Joyner–Halenda (BJH) analysis, GO/MoS_2 is characterized by a uniform mesostructured with narrow pore size distribution with a diameter of ~2.5 nm (Figure 3D).

We believe that GO flakes might serve as building blocks in the self-assembly process triggered by reducing agent L-cysteine. This effect was already observed previously by Xu et al. (2021). During this process, GO is functionalized by sulfur and molybdenum. In the next step, at the temperature of 240°C, the sulfur and molybdenum deposited on the spherical structure of GO reacted, forming MoS_2 sheets evenly distributed in the bulk heterostructure.

Electrochemical measurements

$$MoS_2 + xLi^+ + xe^- \rightarrow Li_xMoS_2 \quad (1)$$

The electrochemical properties of GO/MoS_2 are investigated by means of cyclic voltammetry (CV) and galvanostatic cycling with potential limitation (GCPL). Figure 4A shows the first, second, and tenth cycles of the CV of GO/MoS_2-based electrodes. The initial reductive sweep shows an extended region of activity

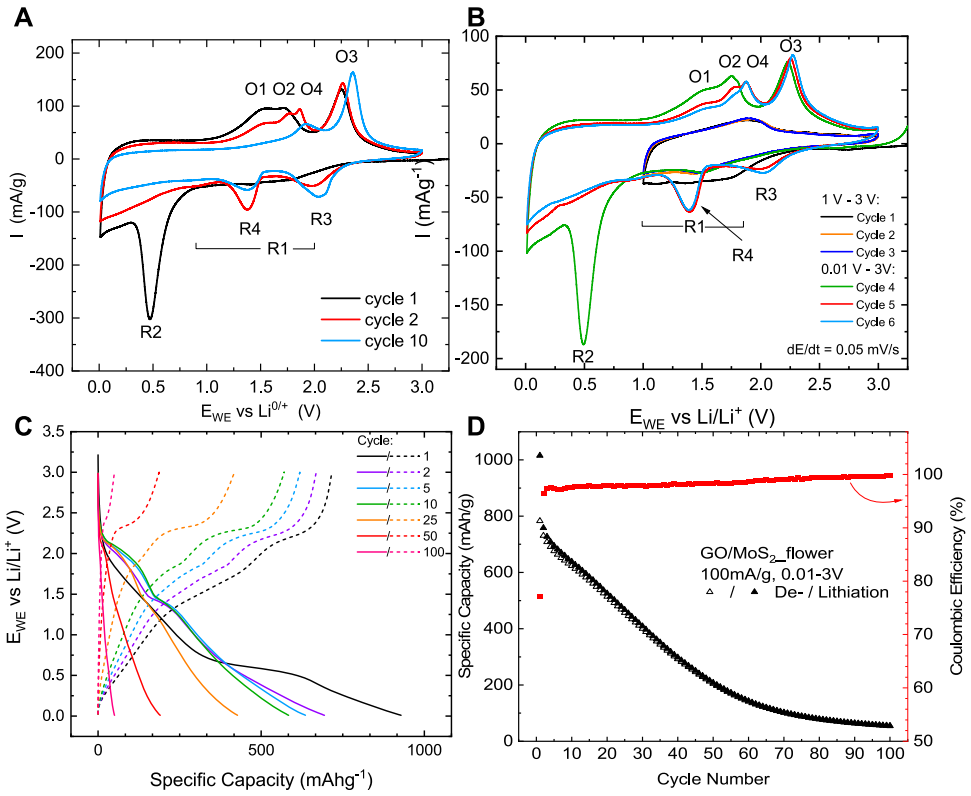

FIGURE 4
(A) Cyclic voltammograms of GO/MoS_2-type electrodes recorded at a scan rate of 0.05 mV/s, **(B)** CV of GO/MoS_2 at a scan rate of 0.05 mV/s in the potential range from 1.0 to 3 V in the first three cycles and subsequently in the potential range of 0.01 to 3 V of cycles 4, 5 and 6. **(C)** Potential profile of galvanostatic cycling of GO/MoS_2 at 100 mA/g between 0.01 and 3 V at specific cycles. **(D)** Specific charge/discharge capacities and associated Coulombic efficiencies during the first hundred cycles studied by GCPL at 100 mA/g.

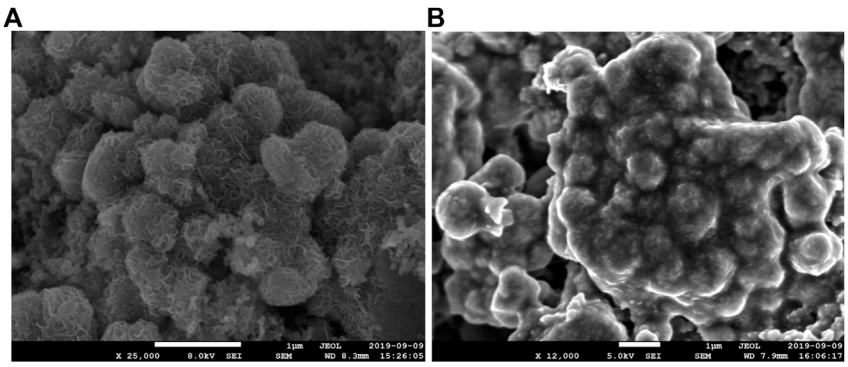

FIGURE 5
SEM images of GO/MoS_2-based electrodes before **(A)** and after 100 times, galvanostatically cycled at 100 mA/g **(B)**.

R1 in the potential range from 1 to 2 V corresponding to the intercalation of Li^+ into the layered structure of MoS_2 (Li et al., 2016) accompanied by a phase transition from trigonal prism structure (2H) into the octahedral structure (1T) (Chang and Chen, 2011; Teng et al., 2016). The absence of a well-defined redox peak agrees with the low crystallinity of MoS_2 in the material, which is also inferred from the XRD data (Figure 3B). The following peak R2 at 0.5 V represents the

subsequent conversion reaction of Li_xMoS_2 into metallic Mo and Li_2S (Li et al., 2016):

$$Li_xMoS_2 + (4 - x)Li^+ + (4 - x)e^- \rightarrow 2Li_2S + Mo. \quad (2)$$

In the first oxidative scan, a broad double peak O1/O2 around 1.5/1.7 V is visible. The corresponding reaction processes are controversially discussed in the literature. On the one hand, O1/O2 has been associated with partial oxidation of Mo, including possible re-formation of MoS_x (Yang et al., 2013; Tang et al., 2014; Wu et al., 2018). However, our CV studies in a restricted potential range (Figure 4B) indicate that peak O1 is linked to the conversion reaction (Eq. 2). The oxidative peak O3 at 2.3 V corresponds to the reversible conversion reaction of Li_2S to elemental S (Li et al., 2016):

$$Li_2S \leftrightarrow S + 2Li^+ + 2e^- \quad (3)$$

The associated reduction peak R3 emerges from the second cycle on at 2.0 V. Figure 4B shows that the reversible de-/lithiation process with the participation of the electrochemical active couple Li_2S/S is enabled by the conversion reaction (Eq. 2), which provides the reactant Li_2S. The main lithium storage mechanism for the following cycles is the reversible sulfur conversion reaction (Eq. 3). This is also visible up to the 100th cycle in the potential profiles (Figure 4C). Starting from the second cycle on, another pronounced reduction peak R4 (1.4 V) and an oxidation peak O4 (1.9 V) emerge. These peaks were also observed by Li et al. (2016), but the underlying processes remain unclear.

The cycling performance of GO/MoS_2-type electrodes studied by GCPL measurements at a current density of 100 mA/g over 100 cycles is displayed in Figure 4D. The dis-/charge capacities in the first cycle are 1,015/783 mA h/g. The capacity loss in the first cycle is mainly attributed to the partially irreversible conversion reaction (Eq. 2) and the formation of a solid electrolyte interface (SEI). Based on the reaction mechanism of Li_2S/S (Eq. 3) with a theoretical capacity of 1,675 mA h/g, for MoS_2, a maximal capacity of 672 mA h/g is expected. Initially, the measured capacities of GO/MoS_2 even exceed this value, suggesting that the complete MoS_2 is involved in the Li^+-ion storage process. The dis-/charge capacities start to decrease constantly from 758/730 mA h/g in the second cycle and stabilize at around 55 mA h/g after 100 cycles. Strong fading effects are expected to arise from mechanical stress associated with the conversion reaction and the dissolution of polysulfides (shuttle effect) during electrochemical cycling. SEM images of a GO/MoS_2-type electrode extracted after the 100th cycle (Figure 5) show that the structure seems to be destroyed after cycling. The same observation has been reported in previous works (Das et al., 2012; Ren et al., 2017a; Ren et al., 2017b), where it is attributed to aggregation of MoS_2 during electrochemical cycling. Moreover, SEM studies confirm that a coating, for example, with TiO_2 or carbon, can prevent structural degradations and thus enhances the cycling stability.

By combining spherical structured MoS_2 nanosheets with graphene oxide, a composite with a large surface area and conductive network is obtained, enabling high accessibility of the active material. The GO/MoS_2 composite initially reaches the full theoretical capacity, but degradation effects lead to poor cycle stability. Comparison with the electrochemical performance of other reported MoS_2/C-composites shows promising options to optimize the cycling stability. The GO/MoS_2 composite studied by Jiao et al. exhibits similar electrochemical properties as the composite studied at hand. N-plasma treatment improves the cycling stability. Another effective strategy to inhibit structural degradation and thus capacity fading is coating MoS_2 with carbon, for example. Das et al. showed that while uncoated MoS_2/C composite delivers a performance like that of the material presented at hand, C-coated MoS_2/C exhibits superior cycling stability. (Das et al., 2012).

Conclusion

In summary, this study presents a facile and reproducible fabrication route of 3D graphene and molybdenum disulfide heterostructure with spherical morphology and their potential application as electrode material in Li-ion batteries. The mechanism of spherical structure formation was proposed. As anode material for Li-ion batteries, the spherical GO/MoS_2 initially delivers an excellent capacity by complete conversion. The high surface area attained by the proposed heterostructure and the presence of graphene oxide, providing a conductive network, enable the high theoretical capacity of MoS_2. Therefore, we believe this material shows considerable promise from both a scientific viewpoint and practical applications.

Data availability statement

The raw data supporting the conclusion of this article will be made available by the authors without undue reservation.

Author contributions

Conceptualization, KW, EM, and RK; methodology and formal analysis, ET,XC and KW; writing–original draft preparation, KW, LS, VA, and ET; writing–review and editing, EM, RK, XC, visualization, KW, ET; funding acquisition, EM, RK, XC. All authors have read and agreed to the published version of the manuscript.

Acknowledgments

The authors are grateful for the financial support from National Science Centre Poland OPUS 10 UMO-2015/19/B/ST8/00648 and Beethoven UMO-2016/23/G/ST5/04200. This

work was partly supported by Deutsche Forschungsgemeinschaft DFG *via* KL 1824/12-1.

Conflict of interest

The authors declare that the research was conducted in the absence of any commercial or financial relationships that could be construed as a potential conflict of interest.

Publisher's note

All claims expressed in this article are solely those of the authors and do not necessarily represent those of their affiliated organizations or those of the publisher, the editors, and the reviewers. Any product that may be evaluated in this article, or claim that may be made by its manufacturer, is not guaranteed or endorsed by the publisher.

References

Chang, K., and Chen, W. (2011). l-Cysteine-Assisted synthesis of layered MoS2/graphene composites with excellent electrochemical performances for lithium ion batteries. *ACS Nano* 5 (6), 4720–4728. doi:10.1021/nn200659w

Chhowalla, M., and Amaratunga, G. A. (2000). Thin films of fullerene-like MoS 2 nanoparticles with ultra-low friction and wear. *Nature* 407, 164–167. doi:10.1038/35025020

Cui, C., Li, X., Hu, Z., Xu, J., Liu, H., and Ma, J. (2015). Growth of MoS2@C nanobowls as a lithium-ion battery anode material. *RSC Adv.* 5, 92506–92514. doi:10.1039/C5RA17992K

Das, S. K., Mallavajula, R., Jayaprakash, N., and Archer, L. A. (2012). Self-assembled MoS2–carbon nanostructures: Influence of nanostructuring and carbon on lithium battery performance. *J. Mat. Chem.* 22 (26), 12988. doi:10.1039/C2JM32468G

David, L., Bhandavat, R., and Singh, G. (2018). MoS2/graphene composite paper for sodium-ion battery electrodes. *ACS Nano* 8 (2), 1759–1770. doi:10.1021/nn406156b

Gao, M.-R., Xu, Y.-F., Jiang, J., and Yu, S.-H. (2013). Nanostructured metal chalcogenides: Synthesis, modification, and applications in energy conversion and storage devices. *Chem. Soc. Rev.* 42 (7), 2986–3017. doi:10.1039/C2CS35310E

Hu, Z., Liu, Q., Sun, W., Li, W., Tao, Z., Chou, S.-L., et al. (2016). MoS2 with an intercalation reaction as a long-life anode material for lithium ion batteries. *Inorg. Chem. Front.* 3 (4), 532–535. doi:10.1039/C5QI00237K

Hummers, W. S., and Offeman, R. E. (1958). Preparation of graphitic oxide. *J. Am. Chem. Soc.* 80, 1339. doi:10.1021/ja01539a017

Ji, S., Kim, S. K., Song, W., Yoon, Y., Myung, S., Lim, J ., et al. (2020). Extraordinary lithium storage capacity and lithiation mechanism of partially amorphous molybdenum sulfide on chemically exfoliated graphene. *Electrochimica Acta* 354, 136636. doi:10.1016/j.electacta.2020.136636

Koroteev, V. O., Stolyarova, S. G., Kotsun, A. A., Modin, E., Makarova, A. A., Shubin, Y., et al. (2021). Nanoscale coupling of MoS2 and graphene via rapid thermal decomposition of ammonium tetrathiomolybdate and graphite oxide for boosting capacity of Li-ion batteries. *Carbon* 173, 194–204. doi:10.1016/j.carbon.2020.10.097

Li, H., Li, W., Ma, L., Chen, W., and Wang, J. (2009). Electrochemical lithiation/delithiation performances of 3D flowerlike MoS2 powders prepared by ionic liquid assisted hydrothermal route. *J. Alloys Compd.* 471 (1-2), 442–447. doi:10.1016/j.jallcom.2008.03.133

Li, D. J., Maiti, U. N., Lim, J., Choi, D. S., Lee, W. J., Oh, Y., et al. (2014). Molybdenum sulfide/N-doped CNT forest hybrid catalysts for high-performance hydrogen evolution reaction. *Nano Lett.* 14 (3), 1228–1233. doi:10.1021/nl404108a

Li, Z., Liu, S., Vinayan, B. P., Zhao-Karger, Z., Diemant, T., Wang, K., et al. (2019). Hetero-layered MoS2/C composites enabling ultrafast and durable Na storage. *Energy Storage Mater.* 21, 115–123. doi:10.1016/j.ensm.2019.05.042

Li, Z., Ottmann, A., Sun, Q., Kast, A. K., Wang, K., Zhang, T., et al. (2019). Hierarchical MoS 2–carbon porous nanorods towards atomic interfacial engineering for high-performance lithium storage. *J. Mat. Chem. A Mat.* 7 (13), 7553–7564. doi:10.1039/C8TA12293H

Li, Z., Ottmann, A., Thauer, E., Neef, C., Sai, H., Sun, Q., et al. (2016). A facile synthesis method and electrochemical studies of a hierarchical structured MoS2/C-nanocomposite. *RSC Adv.* 6 (79), 76084–76092. doi:10.1039/C6RA11214E

Li, Z., Ottmann, A., Zhang, T., Sun, Q., Meyer, H.-P., Vaynzof, Y., et al. (2017). Preparation of hierarchical C@MoS2@C sandwiched hollow spheres for lithium ion batteries. *J. Mat. Chem. A Mat.* 5 (8), 3987–3994. doi:10.1039/C6TA10439H

Liu, C. L., Bai, Y., Zhao, Y., Yao, H., and Pang, H. (2020). MoS2/graphene composites: Fabrication and electrochemical energy storage. *Energy Storage Mater.* 33, 470–502. doi:10.1016/j.ensm.2020.06.020

Liu, Y. M., Zhang, C. L., Cui, J. H., and Wei, W. (2020). Graphene enwrapped molybdenum disulfide for long life rechargeable batteries. *Mat. express* 10, 1358–1363. doi:10.1166/mex.2020.1748

Long, F., Chen, Y., Wu, C. H., Wang, J. L., Mo, S. Y., Zou, Z. G., et al. (2014). Unique three-dimensional hierarchical heterogeneous MoS2/graphene structures as a high-performance anode material for lithium-ion batteries. *IONICS* 27, 1977–1986. doi:10.1007/s11581-021-03936-y

Novoselov, K. S., Geim, A. K., Morozov, S. V., Jiang, D., Zhang, Y., Dubonos, S. V., et al. (2004). Electric field effect in atomically thin carbon films. *Science* 306, 666–669. doi:10.1126/science.1102896

Novoselov, K. S., Jiang, D., Schedin, F., Booth, T. J., Khotkevich, V. V., Morozov, S. V., et al. (2005). Two-dimensional atomic crystals. *Proc. Natl. Acad. Sci. U. S. A.* 102, 10451–10453. doi:10.1073/pnas.0502848102

Ottmann, A., Zakharova, G. S., Ehrstein, B., and Klingeler, R. (2015). Electrochemical performance of single crystal belt-like NH4V3O8 as cathode material for lithium-ion batteries. *Electrochim. Acta* 174, 682–687. doi:10.1016/j.electacta.2015.06.027

Ren, W., Zhang, H., Guan, C., and Cheng, C. (2017). Ultrathin MoS2Nanosheets@Metal organic framework-derived N-doped carbon nanowall arrays as sodium ion battery anode with superior cycling life and rate capability. *Adv. Funct. Mat.* 27 (32), 1702116. doi:10.1002/adfm.201702116

Ren, W., Zhou, W., Zhang, H., and Cheng, C. (2017). ALD TiO2-coated flower-like MoS2 nanosheets on carbon cloth as sodium ion battery anode with enhanced cycling stability and rate capability. *ACS Appl. Mat. Interfaces* 9 (1), 487–495. doi:10.1021/acsami.6b13179

Stephenson, T., Li, Z., Olsen, B., and Mitlin, D. (2014). Lithium ion battery applications of molybdenum disulfide (MoS2) nanocomposites. *Energy Environ. Sci.* 7, 209–231. doi:10.1039/C3EE42591F

Tang, Y., Wu, D., Mai, Y., Pan, H., Cao, J., Yang, C., et al. (2014). A two-dimensional hybrid with molybdenum disulfide nanocrystals strongly coupled on nitrogen-enriched graphene via mild temperature pyrolysis for high performance lithium storage. *Nanoscale* 6 (24), 14679–14685. doi:10.1039/C4NR05519E

Teng, Y., Zhao, H., Zhang, Z., Li, Z., Xia, Q., Zhang, Y., et al. (2016). MoS2 nanosheets vertically grown on graphene sheets for lithium-ion battery anodes. *ACS Nano* 10 (9), 8526–8535. doi:10.1021/acsnano.6b03683

Wang, J., Ma, F., and Sun, M. (2017). Graphene, hexagonal boron nitride, and their heterostructures: Properties and applications. *RSC Adv.* 7, 16801–16822. doi:10.1039/C7RA00260B

Wang, W. W., Guo, S. Z., Zhang, P. L., Liu, J. Z., Zhou, C. C., Zhou, J. J., et al. (2021). Interlayer expanded MoS2/nitrogen-doped carbon hydrangea nanoflowers assembled on nitrogen-doped three-dimensional graphene for high-performance lithium and sodium storage. *ACS Appl. Energy Mat.* 4, 5775–5786. doi:10.1021/acsaem.1c00609

Wieting, T., and Verble, J. (1971). Infrared and Raman studies of long-wavelength optical phonons in hexagonal MoS2. *Phys. Rev. B* 3, 4286–4292. doi:10.1103/PhysRevB.3.4286

Wu, M., Xia, S., Ding, J., Zhao, B., Jiao, Y., Du, A., et al. (2018). Growth of MoS2 nanoflowers with expanded interlayer distance onto N-doped graphene for reversible lithium storage. *ChemElectroChem* 5 (16), 2263–2270. doi:10.1002/celc.201800520

Xiong, P., Ma, R., Sakai, N., Nurdiwijayanto, L., and Sasaki, T. (2018). Unilamellar metallic MoS2/graphene superlattice for efficient sodium storage and hydrogen evolution. *ACS Energy Lett.* 3 (4), 997–1005. doi:10.1021/acsenergylett.8b00110

Xu, M., Wu, T., Qi, J., Zhou, D., and Xiao, Z. (2021). V2C/VO2 nanoribbon intertwined nanosheet dual heterostructure for highly flexible and robust lithium–sulfur batteries. *J. Mat. Chem. A Mat.* 9, 21429–21439. doi:10.1039/D1TA05693J

Yang, L., Wang, S., Mao, J., Deng, J., Gao, Q., Tang, Y., et al. (2013). Hierarchical MoS(2)/polyaniline nanowires with excellent electrochemical performance for lithium-ion batteries. *Adv. Mat.* 25 (8), 1180–1184. doi:10.1002/adma.201203999

Zhang, F., Tang, Y., Liu, H., Ji, H., Jiang, Ch., Zhang, J., et al. (2016). Uniform incorporation of flocculent molybdenum disulfide nanostructure into three-dimensional porous graphene as an anode for high-performance lithium ion batteries and hybrid supercapacitors. *ACS Appl. Mat. Interfaces* 8, 4691–4699. doi:10.1021/acsami.5b11705

Zhang, X., Li, X., Liang, J., Zhu, Y., and Qian, Y. (2016). Synthesis of MoS2@ C nanotubes via the kirkendall effect with enhanced electrochemical performance for lithium ion and sodium ion batteries. *Small* 12 (18), 2484–2491. doi:10.1002/smll.201600043

Zhang, Z., Zhao, H., Teng, Y., Chang, X., Xia, Q., Li, Z., et al. (2018). Carbon-sheathed MoS2 nanothorns epitaxially grown on CNTs: Electrochemical application for highly stable and ultrafast lithium storage. *Adv. Energy Mat.* 8 (7), 1700174. doi:10.1002/aenm.201700174

Zheng, L. X., O'Connell, M. J., Doorn, S. K., Liao, X. Z., Zhao, Y. H., Akhadov, E. A., et al. (2014). Ultralong single-wall carbon nanotubes. *Nat. Mat.* 3, 673–676. doi:10.1038/nmat1216

Zhu, J., Yang, D., Yin, Z., Yan, Q., and Zhang, H. (2014). Graphene and graphene-based materials for energy storage applications. *Small* 10, 3480–3498. doi:10.1002/smll.201303202